Novel heteroanionic titanium oxycarbide photocatalyst for effective congo red degradation and H_2O_2 production

Yathavan Subramanian[1], Anitha Dhanasekaran[1], Lukman Ahmed Omeiza[1], Juliana Haji Zaini[1], John T.S. Irvine[2], Abul K Azad[1*]

[1]*Faculty of Integrated Technologies, Universiti Brunei Darussalam, Gadong BE1410, Brunei*
[2]*The School of Chemistry, University of St Andrews, North Haugh, St Andrews KY16 9ST, United Kingdom.*

[*]Corresponding author: Email: abul.azad@ubd.edu.bn;

Abstract

Combining a rational design strategy with a simple synthetic method to produce an eco-friendly material is an unique challenge in photocatalysis technology. The precedent work reports the successful synthesis of a novel heteroanionic titanium oxycarbide -$TiO_{0.25}C_{0.75}$ (TiOC) photocatalyst through a facile solid-state reaction. Characterization analyses such as SEM, XRD, TEM, EDS, and UV-Vis were carried out to analyze the morphological, structural, and optical properties which play a crucial role in the congo red (CR) degradation and H_2O_2 production process. As synthesized, TiOC demonstrated a moderate CR degradation efficiency of 51 % rate using 1 g/L in 120 min and evolved a minimal amount of H_2O_2 after 90 min (2 mmol) and 120 min (10 mmol) by visible light exposure. The results of CR degradation and H_2O_2 generation reveal that localization of hybridization of O-2p and C-2p orbitals and a more positive conduction band edge of TiOC lead to reduced carrier mobility and, consequently, the high recombination of photogenerated charge carriers. In order to inhibit the recombination of charge carriers, sacrificial reagents such as H_2O_2 and isopropyl alcohol (ISA) were employed in the CR degradation and H_2O_2 evolution processes, respectively. After the addition of sacrificial reagents, the CR removal rate and H_2O_2 evolution rate of TiOC are widely improved to 70 % and 21.5 mmol in 120 min. Furthermore, based on the experimental results, a possible mechanism for CR degradation and H_2O_2 generation using TiOC in the presence of a sacrificial reagent was also proposed. This study may pave the way for the creation of innovative heteroanionic catalysts with better light absorption capacity and less recombination rate for future photocatalysis technology.

Keywords: Photocatalysis; Titanium oxycarbide; Heteroanionic photocatalyst; Congo Red; Hydrogen peroxide generation.

Graphical Abstract:

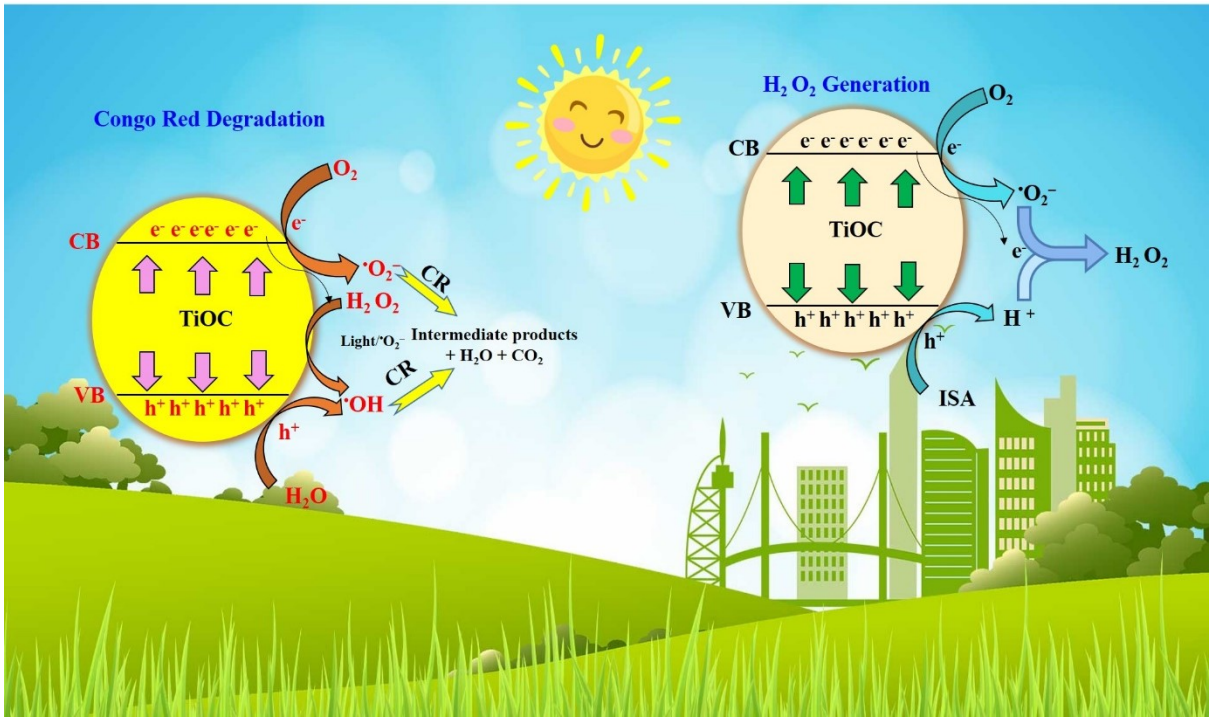

1. Introduction

In the past few decades, research interest has risen in developing materials that can show the capability of both generating greener energy and degrading organic pollutants using visible solar radiation [1], [2]. Mainly, water pollution through industrial processes is a growing concern, as many organic dyes and medical wastes are discharged into water bodies [3]. More specifically, Congo red (CR) dye is a highly hazardous and carcinogenic anionic dye. It is used in the textile, printing, dying, and rubber industries as a colorant. The consumption of CR mixed water causes cancer and mutations in plants, animals, and humans [4], [5]. Therefore, it is of the utmost need to create unique materials & approaches to combat this severe problem to alleviate the pure drinking water shortage. Moreover, the demand for clean and green energy sources in recent years has created many challenges, including the need to find alternatives to conventional energy sources, which cause significant damage to the ecosystem. Based on this demand, Hydrogen peroxide (H_2O_2) was found to be a promising eco-friendly compound that generates greener energy during combustion without producing other toxic compounds. Besides, it possesses good calorific value and oxidation capability and evolves greener products (H_2O and O_2) during combustion [6], [7]. These characteristics made H_2O_2 to play a significant

role in the petrochemical industry, making pulp and papers, sewage treatment for disinfection, etc.,[8], [9]. The anthraquinone (AQ) process is the most widely employed conventional method for generating a large amount of hydrogen peroxide, which possesses few drawbacks, such as the complex process yields toxic by-products and is costlier [10], [11]. While considering these bottlenecks, it is necessary to devise a cost-effective and reliable approach for removing CR from drinking water resources and generating hydrogen peroxide from water using solar radiation.

Therefore, photocatalysis is a viable technique for effective CR removal and hydrogen peroxide production due to its mild reaction conditions, lower energy consumption, and absence of secondary pollutants [12], [13]. It is an emerging approach and has gained much popularity in recent years since it uses safe, cheap materials that harvest a large amount of solar radiation and are easy to fabricate. The materials used in this approach have an excellent capability to promote the reduction and oxidation reactions in the reaction chamber, which plays a vital role in the decomposition of organic pollutants and solar fuel generation [14], [15]. Using these advantages, researchers designed various types of photocatalyst materials for organic pollutants degradation and solar-fuel generation. Initially, traditional photocatalysts such as TiO_2, CdS, Bi_2S_3, etc., have been employed for the decomposition of organic dye and solar-fuels generation such as H_2, H_2O_2, NH_3, etc. [16]–[19]. Furthermore, it has excellent stability, a lower cost, and is non-toxic. However, it faces a lot of bottlenecks, such as a wider band gap, less visible-light absorption nature, photo-corrosion issue, and quick recombination rate [20], [21]. Due to these, a big question arises of whether these traditional photocatalysts have the capacity to meet increasing energy demand and degrade emerging stable pollutants in the future. Hence, researchers viewed heteroanionic materials as a feasible alternative to conventional photocatalysts for future energy generation and water purification techniques due to their superior light absorption capacity, narrower band gap, and improved photo-corrosion resistance [22], [23]. Heteroanionic photocatalysts mainly possess metal cations as the primary elements connected with oxygen and other anion atoms. It has more than one anion in its structure, which provide space for the valence band engineering by careful manipulation of anions [24], [25]. The valence band (VB) of these materials is occupied by mixed hybridized anion-p and oxygen-2p orbitals. Its conduction band (CB) was made up of d^0 or d^{10} orbitals of metal ions; this arrangement induces a narrower band gap with more negative VB than conventional photocatalysts [26], [27]. It can be classified based on the type of anion present in its systems, such as metal oxynitrides, oxysulfides, oxyhalides, and oxycarbides [22].

More specifically, titanium oxycarbide, a heteroanionic photocatalyst, has demonstrated a promising role in photocatalysis applications [28], [29]. It contains a metal ion that is linked to oxygen and carbon atoms. Its electrical and thermal properties can be easily adjustable, and its oxidation resistance, chemical inertness, and photon absorption are exceptional. Its valence band was occupied by hybridized C-2p and O-2p orbitals, while its conduction band is composed of empty d orbitals of metal ions [30]. There are very few reports based on the applications of TiOC in photocatalysis that provided the idea that TiOC exhibits good photocatalytic character towards organic pollutants [31], [32]. It is primarily attributable to the effective separation of photogenerated charge carriers via interfacial charge transfer and its narrower band energy. Moreover, it is believed to have combined characteristics of its oxide and carbide compounds. Hence, we chose titanium oxycarbide as a photocatalyst which will be synthesized through a simple and cost-effective approach and employed for the decomposition of CR and H_2O_2 generation from water using UV- Visible light radiation. We also examined how the photocatalytic efficiency of TiOC over CR degradation and H_2O_2 generation was influenced by its process parameters, such as the amount of catalyst and the presence of sacrificial agents. It has been found from the literature survey that the adoption of TiOC photocatalysts for the decomposition of CR and H_2O_2 generation from the water was not investigated elsewhere.

2. Experimental

2.1. Synthesis of Titanium Oxycarbide

All the compounds were of analytical grade and utilized as received without any additional purification. Titanium oxycarbide was synthesized by blending titanium (II) oxide (TiO) and titanium carbide (TiC) in a mortar with acetone for four hours. The mixed powders were then dried and compressed into pellets using two tons uniaxial press. The resultant pellets were heated in two phases at 1000 °C and 1500 °C for 6 hours, with a heating rate of 5 °C/min in a vacuum atmosphere as shown in Fig. 1. The chemical reactions involved in the formation of TiOC have been represented as follows:

$$0.25(TiO) + 0.75(TiC) \rightarrow TiO_{0.25}C_{0.75} \quad (1)$$

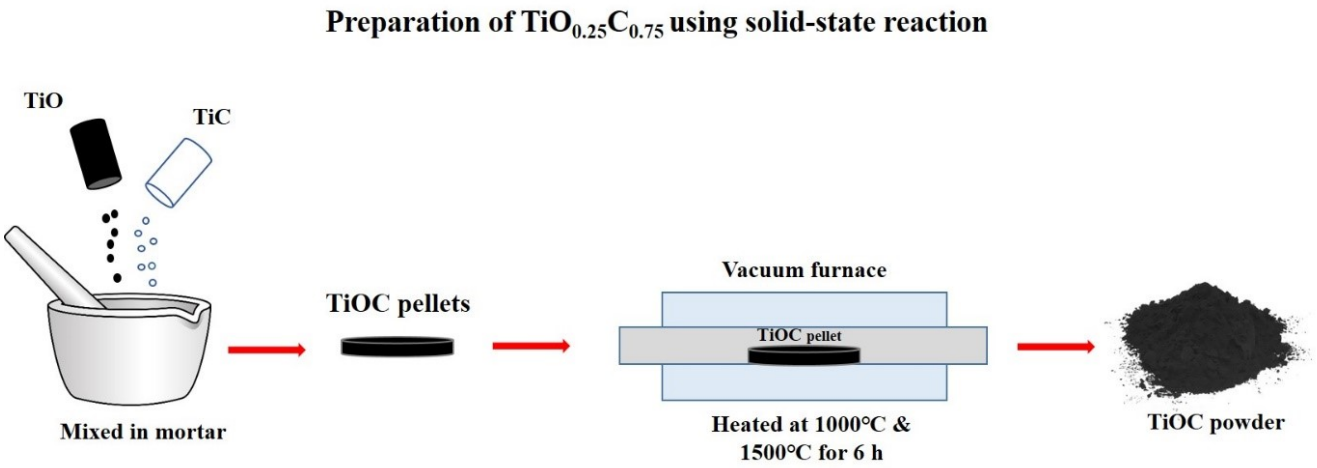

Fig. 1 Preparation of $TiO_{0.25}C_{0.75}$ using solid-state reaction

2.2. Material Characterization

The crystalline structure and morphology feature of synthesized photocatalysts was studied using X-ray diffraction (XRD, PANalytical X'accelerator, $\lambda = 0.15406$ nm) and scanning electron microscope (SEM, JEOL JSM-5600) and a transmission electron microscope (TEM, JEOL-2010). Elemental mapping of the synthesized samples was observed using energy dispersive X-ray spectroscopy (EDX) attached to the SEM instrument. The optical characteristics were calculated using the ultraviolet−visible diffuse absorbance spectrum (UV–Vis DRS) on a JASCO V-670 UV-Vis spectrophotometer.

2.3. Photodegradation test of CR

The photocatalytic character of TiOC was examined on the degradation of CR in an aqueous medium under visible light irradiation. A stock solution of congo red (20 mg/l) was prepared by dissolving CR dye in one liter of deionized water. Then, different concentrations (0.25, 0.50, 0.75, and 1 g/mL) of TiOC photocatalysts were mixed in 100 ml of CR solution. The TiOC-suspended CR solution was treated in the dark for 1 hour in order to achieve the adsorption-desorption equilibrium. After reaching the equilibrium, the dark-treated solution was exposed to the 300 W Xenon light source in the photocatalytic chamber (CAE-HXF 300). The relative concentration of CR in the light-treated solution was evaluated using a Shimadzu UV–vis spectrophotometer at every interval of 30 min.

2.4. Photocatalytic H_2O_2 production test

For the hydrogen peroxide generation test, 50 mg of TiOC photocatalysts were added to 100 mL of deionized water. Then the prepared solution was kept under a 300 W Xenon light source. The generation of H_2O_2 was calculated based on redox titration with $KMnO_4$ as per the previously reported method [33]–[35]. During the photocatalytic reaction, 1 mL of solution was withdrawn from the reaction chamber at every 30 min intervals and purified using a 0.45 µm filter. Then 1 mL purified solution, 2 mL $KMnO_4$ solution (40 mM), and 1 mL H_2SO_4 solution (1 M) were mixed together and held for 3 minutes to make the $KMnO_4$ reduced into $MnSO_4$ by H_2O_2. To determine how much $KMnO_4$ was used in a reaction, the intensity of the light absorbed by the solution at 525 nm was measured at various reaction times. Based on the following equation & formula, the concentration of the generated H_2O_2 can be determined.

$$2\ MnO_4^- + 5\ H_2O_2 + 6H^+ \rightarrow 2\ Mn^{2+} + 5\ O_2 \uparrow + 8\ H_2O \quad (2)$$

$$C_{H_2O_2} = \frac{5}{2} \times \frac{C_{KMnO_4} \times V_{KMnO_4}}{V_{H_2O_2}} \quad (3)$$

3. Results and Discussion

3.1. Powder XRD analysis on Titanium Oxycarbide

X-ray diffraction patterns of TiOC were measured in the 2Θ range from 30° to 80° at a scan rate of 1^0/min, as shown in Fig. 2. The synthesized TiOC depicts the moderately intense peak, confirming the formation of well-crystalline pure phase. It clearly reveals that the XRD patterns of TiOC are well-matched with the standard JCPDS files of TiO and TiC as shown in Fig. 1 [36]. It provides a confirmation that synthesized TiOC has a cubic structure with space group Fm-3m. Mainly, all the peaks of $TiO_{0.25}C_{0.75}$ have shifted and broadened a little towards higher 2θ values, which provides an additional clue for the addition of the carbon atom in the TiO structure. A similar kind of observation was reported in earlier research works on the TiOC [37], [38]. In addition, no other satellite peaks were found in the XRD pattern confirming the purity of the synthesized TiOC photocatalysts.

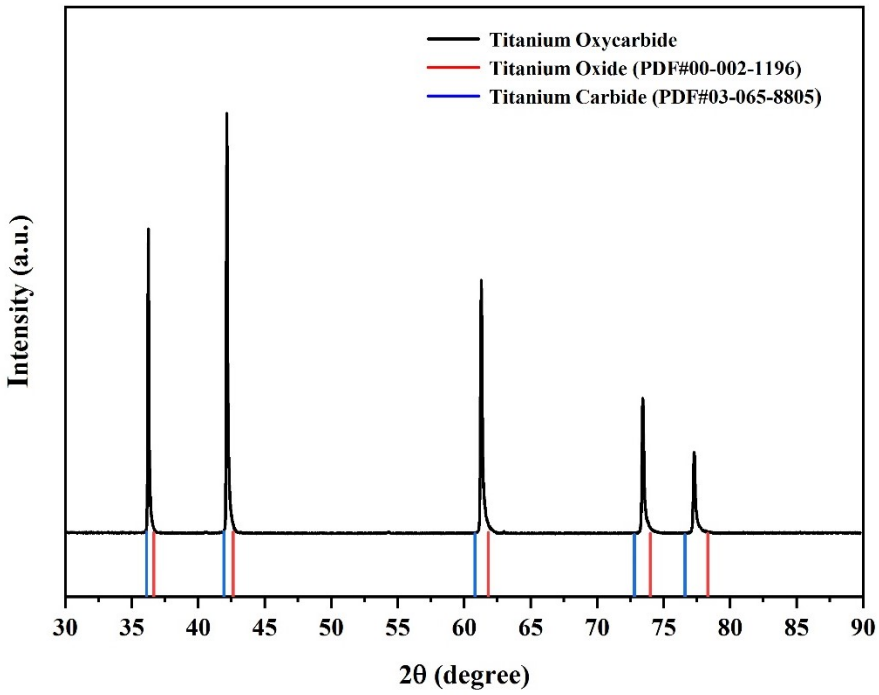

Fig. 2 XRD patterns of $TiO_{0.25}C_{0.75}$ matching with standard JCPDS files of TiO (red) and TiC (blue)

With the help of Williamson-Hall (W-H) formulas [39], the crystalline size and strain of the prepared $TiO_{0.25}C_{0.75}$ photocatalysts have been calculated, as shown in Fig. 3. It has been found that TiOC possesses a large crystalline size and with less strain in it (Table 2.). This may be due to the decrease in crystalline defects and higher synthesis temperature applied for $TiO_{0.25}C_{0.75}$.

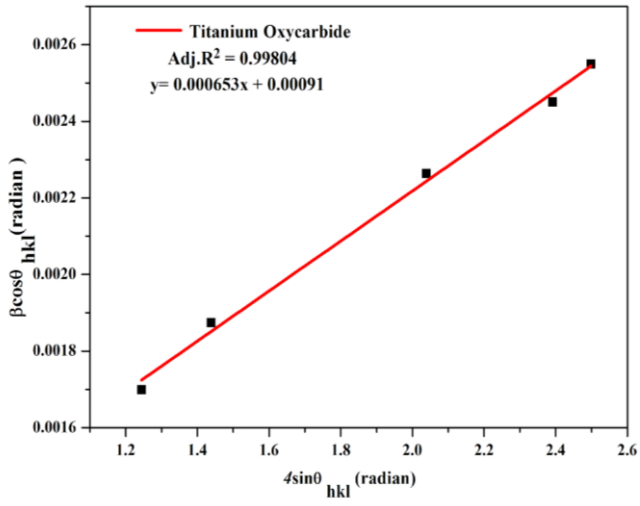

Fig. 3 Williamson-Hall (W-H) analysis for the $TiO_{0.25}C_{0.75}$.

Table 1 Crystalline strain and sizes of titanium oxycarbide

Sl. No.	Sample Name	Sintering temperature (°C)	Crystalline Size (nm)	Strain (No unit)
1	Titanium oxycarbide ($TiO_{0.25}C_{0.75}$)	1500	~152 nm	6.53×10^{-2}

3.2. Scanning and Transmission Electron Microscopy (SEM &TEM)

It is believed that the surface morphology feature of the prepared TiOC plays a dominant role in improving its photocatalytic character. Therefore, the surface morphology of synthesized TiOC was captured using SEM, as shown in Fig. 4 (a).

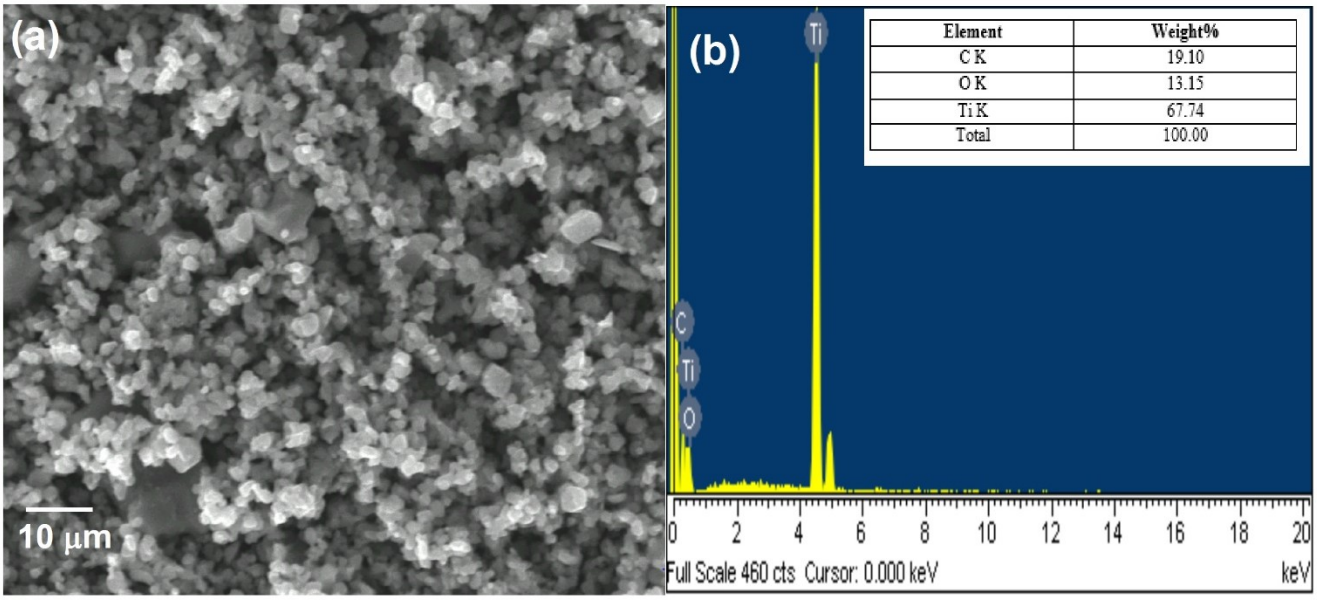

Fig. 4 (a) SEM image and (b) Elemental mapping of prepared $TiO_{0.25}C_{0.75}$ photocatalysts

It has been found that the TiOC surface was made up of uniformly distributed porous and spherical-shaped particles without much agglomeration. Moreover, the higher temperature supplied during the synthesis process help to create a wider surface area with a large crystalline size in TiOC, which induces facial migration of excited electrons and holes to participate in succeeding photocatalytic reactions. Furthermore, it makes a strong interface between the different anions in TiOC, acting as the charge carrier transfer channel. For instance. Negi et al. observed similar observations when carbon was doped in the titanium dioxide structure, which supports the reduction of its agglomeration behavior and provides a wider surface area [40]. It significantly increased the degradation efficiency of C-TiO_2 towards the methylene blue dye. Moreover, the SEM image of the C-TiO_2 closely matches the surface morphology of $TiO_{0.25}C_{0.75}$ found in our observations. The elemental mapping using energy-dispersive X-ray analysis (EDX) also confirmed the fact that elements such as Ti, O, and C are uniformly distributed throughout the sample, as shown in Fig. 4 (b). The TEM images and selected area electron diffraction (SAED) pattern for the synthesized $TiO_{0.25}C_{0.75}$ photocatalyst are displayed in Fig.5 (a) & (b). These observations again confirmed the phase purity of the $TiO_{0.25}C_{0.75}$ photocatalysts, as discussed in the XRD analysis.

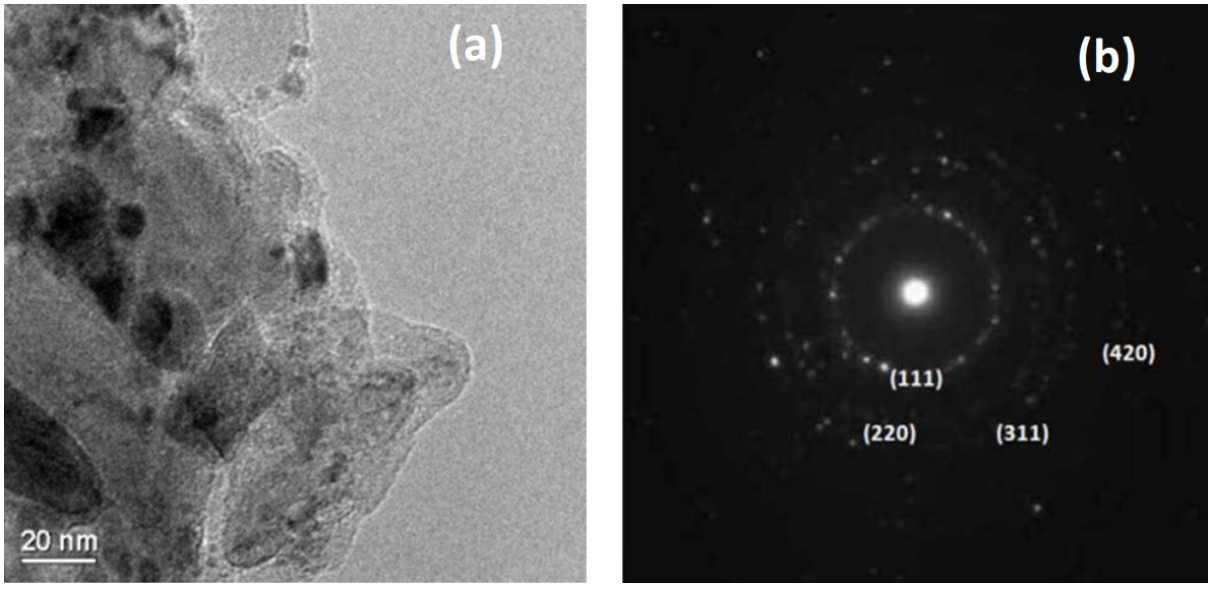

Fig. 5 (a) TEM image of the synthesized $TiO_{0.25}C_{0.75}$ photocatalysts, along with its (b) SAED pattern

3.3. UV-Vis-NIR analysis on Titanium Oxycarbide

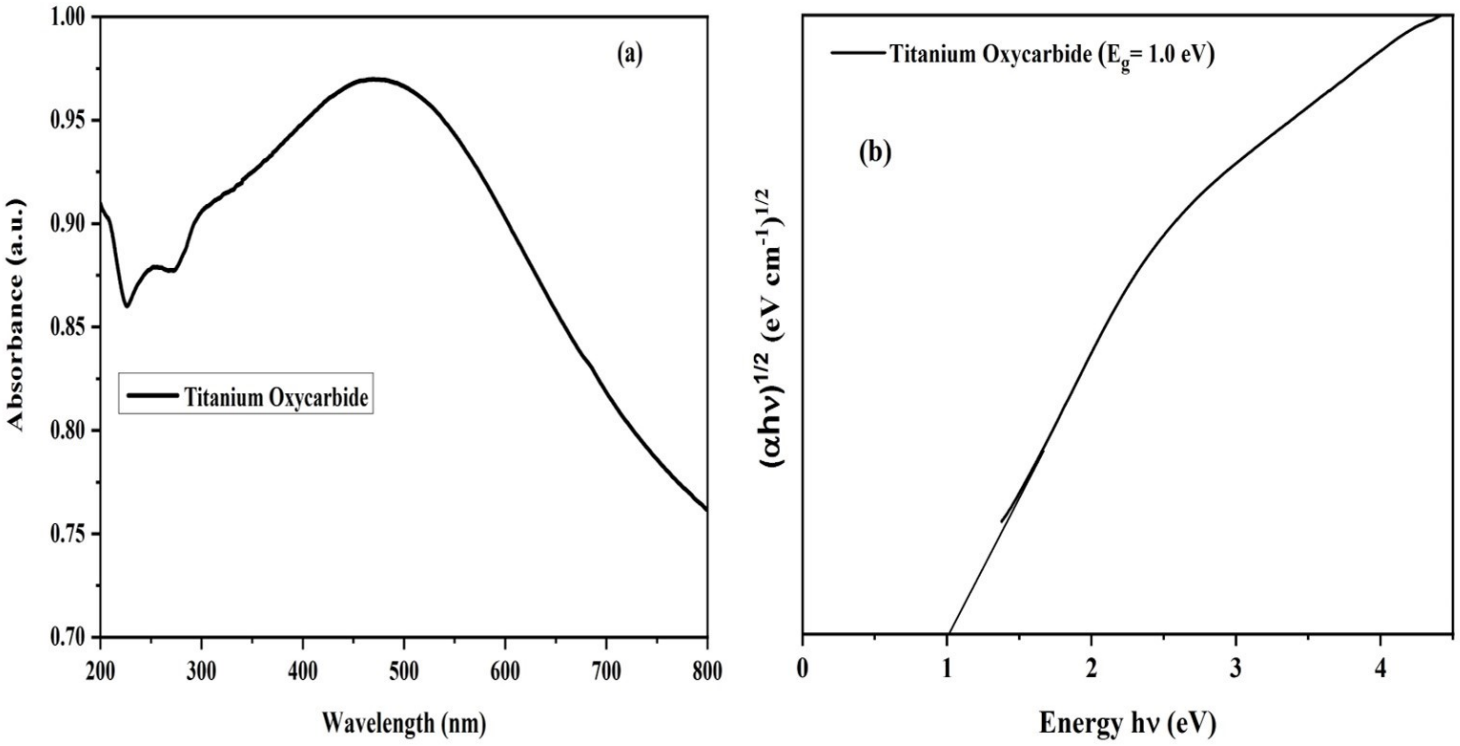

Fig. 6 (a) represents the UV-Vis absorption spectra of synthesized TiOC photocatalysts and (b) its Tauc plot

The optical and energy band gap characteristics of the synthesized TiOC were analyzed using UV–Vis absorption spectra and its tauc plot. On observing Fig 6 (a), it has been found that the absorption edge of TiOC was exhibited around 490 nm and possessed good light absorption characteristics. The band-gap energy (E_g) of TiOC was computed using the Kubelka-Munk (KM) function [41], [42], and its tauc plot is shown in Fig. 6 (b). It represents TiOC possesses narrower band gap energy (Eg) value of 1.0 eV. It was primarily obtained by an upward shift of the VB maximum, not by moving the CB maximum downward, and also by strong hybridization between the C-2p and O-2p orbitals. Moreover, the VB of the TiOC was occupied by mixed C-2p and O-2p orbitals, while its CB is composed of d-orbitals of Ti-ions. A similar kind of band gap reduction was also observed by Negi et al. in C-TiO_2 structure [40]. This kind of electronic arrangement exhibits suitable band edge positions in TiOC, which is crucial in promoting the reduction and oxidation reactions during the decomposition of CR and H_2O_2 generation.

3.4. Photocatalytic Degradation activity of Titanium Oxycarbide

The photocatalytic behavior of TiOC was assessed by observing the degradation of the CR in an aqueous solution under UV–visible light illumination. The CR was more stable under UV-Vis illumination when no photocatalyst was employed. Then TiOC photocatalysts of different concentrations were suspended in the prepared CR and kept in the dark environment to obtain adsorption-desorption equilibrium. After equilibrium had been attained, the dark-treated solution was exposed to UV-Vis light for illumination. The absorption spectra of the light-treated solution were recorded at regular intervals of 30 min with the help of a UV-Vis spectrophotometer. Most importantly, we examined the influence of the process parameters on the CR degradation activity, such as the amount of catalyst and the presence of sacrificial agents. The CR degradation efficiencies and its pseudo-first-order kinetics (Langmuir–Hinshelwood model) of TiOC can be determined using the following formulas [43], [44];

$$\text{Efficiency, } \eta(\%) = \frac{(C_0 - C_t)*100}{C_0} \quad (4)$$

$$ln(C_0/C_t) = kt \quad (5)$$

Where, C_0 and C_t are the concentrations of CR at times 0 and t, respectively, under UV-Vis light exposure; $'k'$ is the pseudo-first-order rate constant of photodegradation (min^{-1}) of CR degradation.

Initially, the effect of catalyst loading on photocatalytic degradation of congo red was studied by varying the amount of TiOC as 0.25 g/L, 0.50 g/L, 0.75 g/L, and 1 g/L. The photocatalytic degradation against time is shown in Fig. 7 (a). From the figure, the concentrations of CR gradually decreased with an increase in the TiOC catalyst. The maximum CR degradation efficiency of TiOC was observed at 1 g/L, which took only 120 min to degrade 55% of CR. Similarly, at 0.25 g/L, 0.50 g/L, and 0.75 g/L of TiOC, it degraded 23%, 46%, & 50% at 120 min, respectively. The CR degradation efficiency for various TiOC photocatalyst amounts has been calculated using equation (4) as plotted in Fig. 7 (b). It is clearly evident that at higher doses of catalyst, more active sites were created on the surface of TiOC due to the massive absorption of light, which led to the creation of an excessive amount of hydroxyl radicals during the degradation of CR. Similarly, the first-order reaction kinetics of CR degradation has been

computed for various TiOC amounts. Its linear fitting has been plotted as Fig. 7(c), and its R^2 values have been tabulated in Table 2.

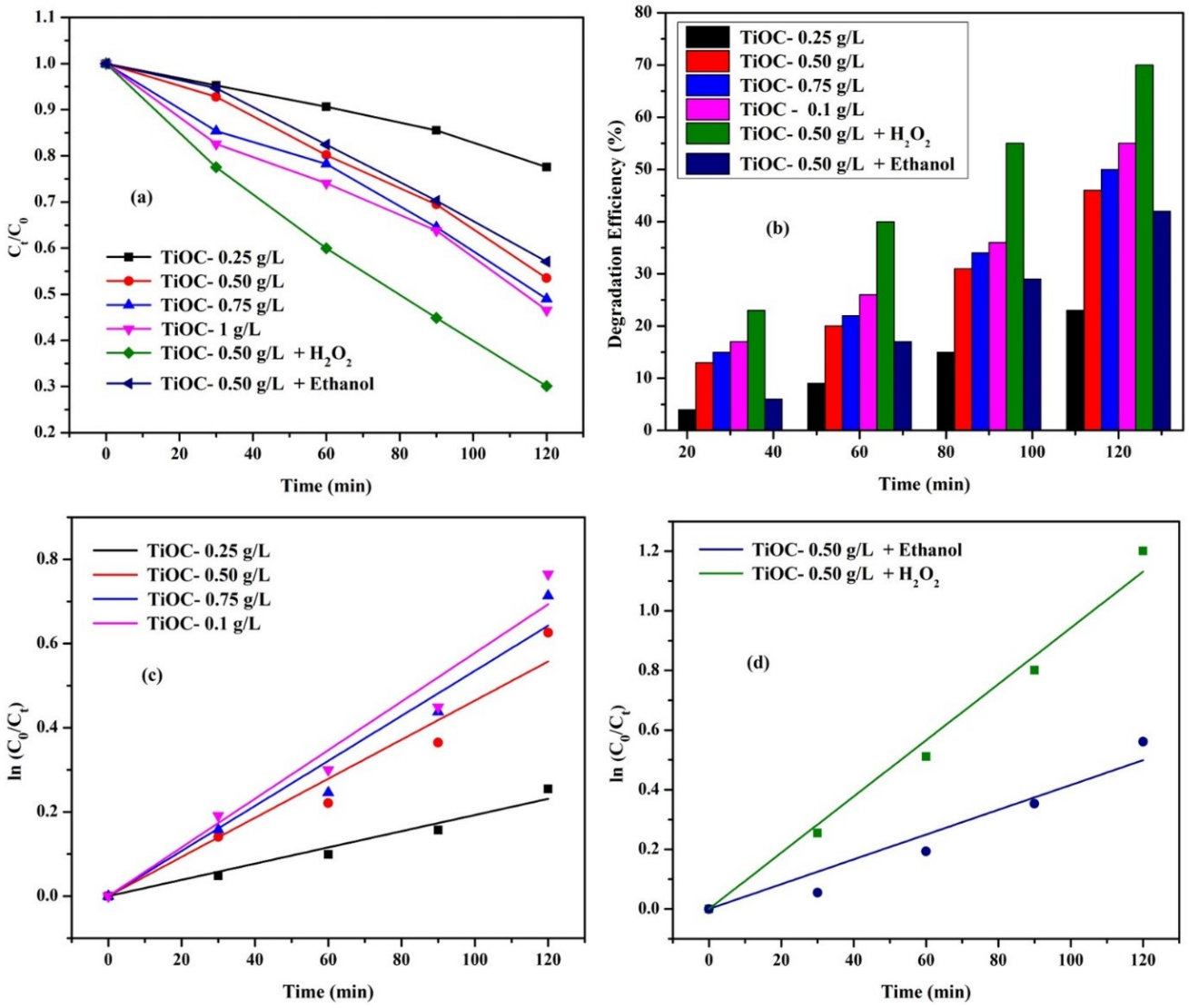

Fig. 7 (a) Comparison of the photocatalytic CR degradation rates using different amounts of TiOC photocatalyst and in the presence of sacrificial reagents; (b) its degradation efficiency; (c) & (d) pseudo-first-order kinetics of the photocatalytic CR degradation rates using different amounts of TiOC photocatalyst and in the presence of sacrificial reagents.

Based on the above results, it has been found that the TiOC showed average CR degradation efficiency even at a higher amount of catalysts compared to commercial photocatalysts. It may be due to the quick recombination of photogenerated electron-hole charge carriers. Therefore, we utilized electron sacrificial reagents such as hydrogen peroxide to investigate the effects of charge carrier separation on photocatalytic efficiency. Hence, we dispersed 1 ml of H_2O_2 (1 mmol) and 0.50 g/L of TiOC into the 100 ml of the prepared CR solution. Surprisingly, after the addition of H_2O_2, we observed the MB decomposition increased to 70%, which performed even better than the CR solution with 1 g/L, and it is degradation characteristics can be seen in Fig. 7(a), (b) & (d). This is because when H_2O_2 was added to the CR solution, the photogenerated electrons on the TiOC surface were captured by electron sacrificial reagents. It automatically reduces the charge carrier recombination rate and provides sufficient time for the holes in the VB to oxidize the water molecules to create potent hydroxyl radicals (•OH). In addition to this, the strong CR adsorption on the TiOC photocatalysts could also play a crucial role in improving the photodegradation efficiency.

Similarly, we also examined the role of the photogenerated holes in the degradation of CR; to analyze this fact, we mixed 1 ml of the ethanol into the prepared CR solution along with 0.50 g/L of TiOC. The CR degradation characteristics of TiOC using ethanol were plotted in Fig. 7 (a),(b) & (d). It was observed that the CR removal rate of TiOC decreased after the inclusion of ethanol. It clearly states that the photogenerated holes of TiOC were entirely consumed by ethanol for its self-degradation to generate CH_3CHO and $2H^+$ ions. Overall, the photogenerated holes of TiOC played a vital role during the decomposition of the CR. A similar kind of experimental observation was observed by Xinjian Xie et al. during the decomposition of organic pollutant MB using $CuWO_4$. They used various sacrificial reagents to suppress the effect of the quick recombination rate of charge carriers [45].

Table 2: Pseudo-first-order kinetics of different amounts of TiOC and in the presence of H_2O_2 and Ethanol.

Sl. No.	Sample code	**Pseudo-first-order kinetics**			**CR degradation efficiency**
		Slope k (min^{-1})	Standard Error	R^2 value	
1	**TiOC (0.25 g/L)**	0.00193	0.0001	0.98524	23%
2	**TiOC (0.50 g/L)**	0.00464	0.0003	0.97696	46%

3	**TiOC (0.75 g/L)**	0.00535	0.0003	0.9797	50%
4	**TiOC (1 g/L)**	**0.00578**	**0.0003**	**0.98272**	**55%**
5	**TiOC (0.50 g/L) + H_2O_2**	**0.00943**	**0.0003**	**0.99438**	**70%**
6	**TiOC (0.50 g/L) + Ethanol**	0.00416	**0.0003**	**0.96772**	42%

3.5. Photocatalytic H_2O_2 generation using Titanium Oxycarbide

Photocatalytic H_2O_2 generation rates on TiOC photocatalysts have been measured every 30 min with/without the addition of the sacrificial reagent such as Isopropyl Alcohol (ISA) under visible light irradiation. In order to make the calibration curves, the absorption curve was evaluated for different volumes of $KMnO_4$ ml (0.2 to 2 ml) which was mixed with one ml of H_2SO_4 and 2 ml of H_2O and held for 3 min. Then a linear fitting plot was made based on the absorbance value absorbed at 523 nm, as shown in Fig. 8 (a) & (b). Initially, the H_2O_2 evolution rate for TiOC was evaluated without adding ISA under visible light radiation. It produced a minimal amount of H_2O_2, such as 2 mmol and 10 mmol, after 90 and 120 min of visible light irradiation, respectively, as shown in Fig. 8 (c). It indicates that pure TiOC is minimally active under UV-Visible light irradiation. This was reasonably anticipated because the photogenerated electrons in the CB of TiOC do not possess enough reduction potential to drive the proton reduction reaction. This is because the CB edge position of the TiOC (0.4 eV) is more positive when compared to the standard redox potential required for the water decomposition and possesses a quick recombination rate of charge carriers. These results confirmed once again that TiOC was capable of showing better photocatalytic character only after 120 min of light exposure. It was clearly observed even during the photodegradation of CR using different concentrations of the TiOC photocatalyst.

Interestingly, the H_2O_2 evolution rate of TiOC has been significantly improved after adding 2ml of ISA as a sacrificial agent. ISA-loaded TiOC produced a good amount of H_2O_2 of 7.5 mmol at 30 min of light irradiation. Upon the completion of 120 min, the H_2O_2 production rate increased to 21.5 mmol of H_2O_2, which doubled the amount of H_2O_2 evolution rate as compared to the reaction without ISA and is shown in Fig. 8 (d). Therefore, the H_2O_2 evolution rate of

TiOC can be increased further only after adding sacrificial reagents, which react irreversibly with the photogenerated holes to enhance electron/hole separation efficiency.

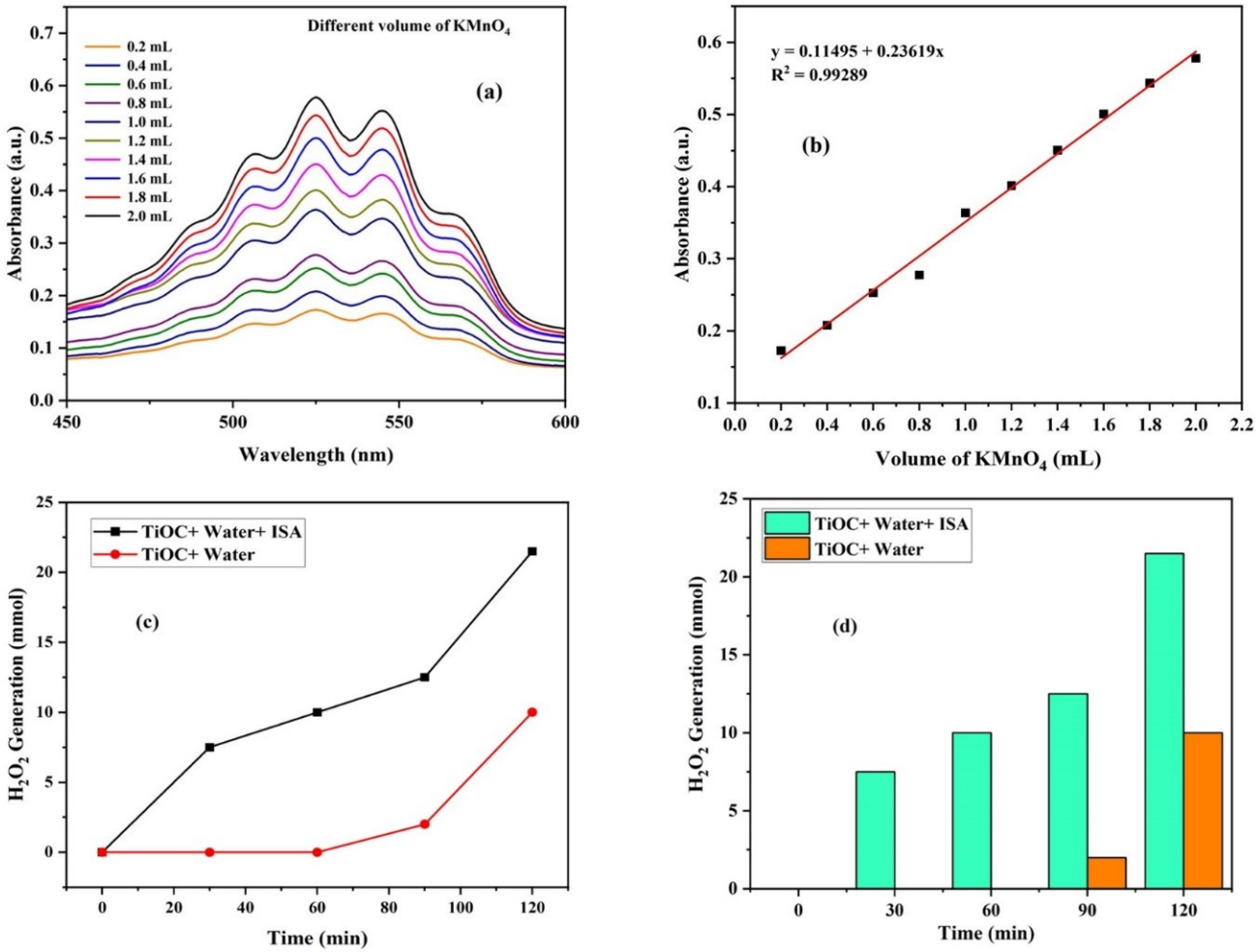

Fig. 8 (a) UV-Vis absorption spectra of 40 mM $KMnO_4$ in aqueous solution with different solution volumes and (b) its linear fitting; (c) & (d) Comparison the photocatalytic H_2O_2 evolution rate of TiOC with/without the presence of ISA.

3.6. Possible mechanism of the photocatalytic CR degradation and H_2O_2 generation using TiOC

The photocatalytic behavior of any compound can be proposed based on its CB and VB edge arrangements. The CB and VB edge positions of TiOC can be determined using the Mulliken electronegativity method in order to present the photocatalytic mechanism that occurred during

the degradation of CR and H_2O_2 generation. This method employs two equations to calculate the valence (E_{VB}) and conduction band (E_{CB}) edge positions of TiOC [3], [44].

$$E_{CB} = X - 4.5\ (E_e) - E_g/2 \quad (6)$$

$$E_{VB} = E_{CB} + E_g \quad (7)$$

Where, X (~5.37 eV) and E_g (~1.0 eV) is the electronegativity and band gap energy value of the TiOC; E_e is the energy of a free electron on a hydrogen scale (4.5 eV).

Based on this technique, the CB and VB edges of TiOC were determined to be 0.4 eV and 1.4 eV, respectively. The acceptable photocatalytic character exhibited by TiOC in the presence of the sacrificial reagents can be attributed to the following factors:

During the CR degradation process, the TiOC absorb light radiation larger/ equal to its band gap energy and encourages the creation of the electron-hole charge carriers and migrates their electrons from the valence band of TiOC surface to its conduction band, which acts as the trapping site of electrons. In general, the electrons in CB generate superoxide radical ($\bullet O_2^-$) by reacting with molecular oxygen in the reaction chamber. Then the superoxide radicals ($\bullet O_2^-$) react with water molecules to create •OH. At the same time, photogenerated holes in the VB oxidize OH^- to produce •OH radicals.

When the H_2O_2 is introduced as a sacrificial reagent in the reaction chamber, it helps to create more hydroxyl radicals either by interaction with light radiation, superoxide anion, or by reacting the electrons from CB of TiOC as shown in equations (13-15). Hydroxyl radical (•OH) and superoxide radical ($\bullet O_2^-$) are the main species that degrade CR into carbon dioxide and water molecules under light illumination. Moreover, this reaction reduces the recombination rate of the charge carriers by providing sufficient charge separation. It induces a strong internal electric field between the different anions in TiOC, and increases the photocatalytic CR degradation efficiency.

The chemical reactions involved in the degradation of CR using TiOC in the presence of H_2O_2 are as follows;

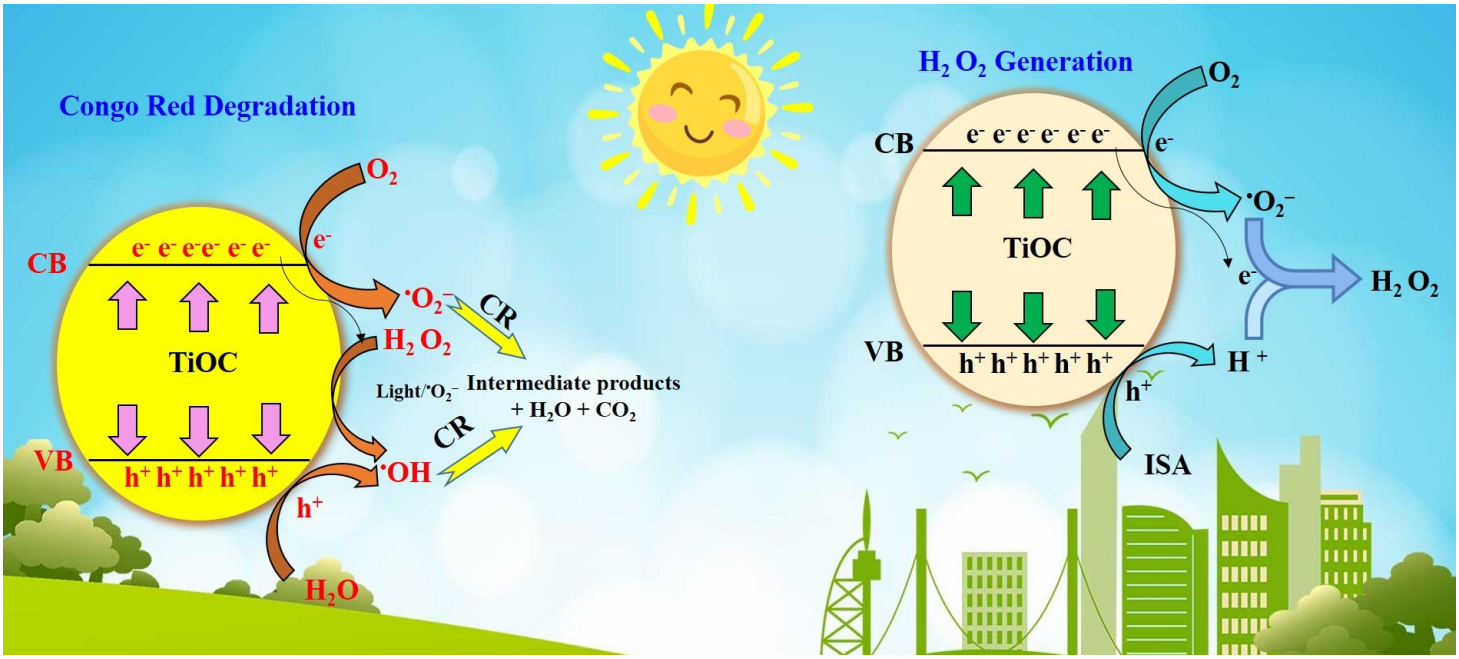

Fig. 9 The possible mechanism of photocatalytic congo red degradation & H_2O_2 production from TiOC photocatalyst.

$$TiOC + hv\ (light) \rightarrow e^- + h^+ \quad (8)$$

$$TiOC\ (e^-)_{CB} + O_2 \rightarrow {}^\bullet O_2^- \quad (9)$$

$${}^\bullet O_2^- + 2H_2O \rightarrow 2\ {}^\bullet OH + 2OH^- \quad (10)$$

$$OH^- + H+ \rightarrow {}^\bullet OH \quad (11)$$

$$TiOC\ (h^+)_{VB} + 2H_2O \rightarrow TiOC + {}^\bullet OH + H^+ \quad (12)$$

$$H_2O_2 + hv\ (light) \rightarrow 2\ {}^\bullet OH \quad (or) \quad (13)$$

$$H_2O_2 + O_2^- \rightarrow {}^\bullet OH + OH^- + O_2 \quad (or) \quad (14)$$

$$H_2O_2 + TiOC\ (e^-)_{CB} \rightarrow OH^- + {}^\bullet OH \quad (or) \quad (15)$$

$${}^\bullet O_2^- + CR \rightarrow \text{intermediate products} + \text{degradation } (H_2O + CO_2) \text{ products} \quad (16)$$

$^{\bullet}OH + CR \rightarrow$intermediate products + degradation ($H_2O + CO_2$) products (17)

In addition, we also proposed a possible mechanism of H_2O_2 generation using TiOC as a two-step single-electron O_2 reduction reaction, as shown in Fig 9. When the TiOC is exposed to visible light radiation, it automatically generates electron–hole charge carriers. The electrons in the CB of TiOC react with molecular oxygen in the reaction chamber to create superoxide radicals. The holes at the VB of TiOC oxidize the ISA to produce the protons. Then these superoxide radicals and protons react with another electron to generate the H_2O_2. The reaction involved during the H_2O_2 evolution reaction using TiOC can be described as follows [46].

$TiOC + hv \rightarrow e^- + h^+$ (18)

$TiOC\ (e^-)_{CB} + O_2 \rightarrow {}^{\bullet}O_2^-$ (19)

$TiOC\ 2\ (h^+)_{VB} + CH_3CH(OH)CH_3 \rightarrow CH_3COCH_3 + 2H^+$ (20)

$O_2^- + 2H^+ + e^- \rightarrow H_2O_2$ (21)

Therefore, the supplying & separating of sufficient electrons and holes in TiOC will automatically trigger the redox reactions in it, leading to enhanced photocatalytic activity.

4. Conclusions

In summary, titanium oxycarbide photocatalysts have been successfully prepared by supplying two calcination temperatures such as 1000 °C and 1500 °C, for 6 hours. The XRD, SEM, TEM and elemental mapping confirmed the purity of the TiOC. It was found that the synthesized TiOC photocatalysts possess maximum absorption edge at 500 nm and exhibited a low band gap energy of 1.0 eV due to the formation of hybridized C-2p and O-2p orbitals at the valence band. Initially, TiOC demonstrated a moderate CR degradation efficiency of 51 % using 1 g/L in 120 min and evolved a minimal amount of H_2O_2 after 90 min and 120 min of visible light exposure. The results of CR degradation and H_2O_2 generation without any sacrificial agent reveal that due to more positive CB position than the standard H^+/H_2O reduction potential and localization of hybridization of O 2p-orbitals and C 2p-orbitals lead to the reduced carrier mobility and improved quick recombination of photogenerated charge carriers. But in the presence of sacrificial reagents such as H_2O_2 and ISA, the CR removal rate and H_2O_2 evolution rate of TiOC are significantly improved to 70% and 21.5 mmol in 120 min, respectively. This enhancement in the photocatalytic activity is due to the suppression of the recombination of

photogenerated charge carriers. It provides sufficient time to a large number of hydroxyl radicals (•OH) and H+ ions after the addition of sacrificial reagents. Novel titanium oxycarbide photocatalysts with good light absorption character and less recombination rate of the charge carriers by adding dopant/formation of heterostructures with other visible-light semiconductors can be done in future. To our knowledge, it is the first investigation of the photocatalytic activity of TiOC through the degradation of congo red and H_2O_2 generation experiment under UV-Visible light radiation.

CRediT authorship contribution statement

Yathavan Subramanian: Investigation, Methodology, Performed experiments, Writing – original draft; **Anitha Dhanasekaran:** Investigation, Writing – review & editing; **Lukman Ahmed Omeiza:** Contributed reagents, materials, analysis tools or data; **Juliana Haji Zaini**: Visualization, Writing – review & editing, Conceptualization, Resources, Supervision; .**John T.S. Irvine:** Conceptualization, Resources, Supervision, Visualization, Review & Editing: **Abul Kalam Azad:** Visualization, Writing – review & editing, Conceptualization, Resources, Supervision.

Declaration of competing interest

The authors declare no conflict of interest.

Acknowledgment

The authors, Yathavan Subramanian, Anitha Dhanasekaran and Lukman Ahmed Omeiza would like to thank the Universiti of Brunei Darussalam for the UGS scholarship for their PhD research.

References:

[1] M. B. Tahir, A. M. Asiri, and T. Nawaz, "A perspective on the fabrication of heterogeneous photocatalysts for enhanced hydrogen production," *Int J Hydrogen Energy*, vol. 45, no. 46, pp. 24544–24557, Sep. 2020, doi: 10.1016/j.ijhydene.2020.06.301.

[2] D. Chen *et al.*, "Photocatalytic degradation of organic pollutants using TiO2-based photocatalysts: A review," *J Clean Prod*, vol. 268, p. 121725, Sep. 2020, doi: 10.1016/j.jclepro.2020.121725.

[3] Y. Subramanian *et al.*, “Efficient degradation of endocrine-disrupting compounds by heterostructured perovskite photocatalysts and its correlation with their ferroelectricity,” *New Journal of Chemistry*, vol. 46, no. 24, pp. 11851–11861, 2022, doi: 10.1039/D2NJ00785A.

[4] M. Hernández-Zamora, F. Martínez-Jerónimo, E. Cristiani-Urbina, and R. O. Cañizares-Villanueva, “Congo red dye affects survival and reproduction in the cladoceran Ceriodaphnia dubia. Effects of direct and dietary exposure,” *Ecotoxicology*, vol. 25, no. 10, pp. 1832–1840, Dec. 2016, doi: 10.1007/s10646-016-1731-x.

[5] P. O. Oladoye, M. O. Bamigboye, O. D. Ogunbiyi, and M. T. Akano, “Toxicity and decontamination strategies of Congo red dye,” *Groundw Sustain Dev*, vol. 19, p. 100844, Nov. 2022, doi: 10.1016/j.gsd.2022.100844.

[6] A.-L. Chang, V.-H. Nguyen, K.-Y. A. Lin, and C. Hu, “Selective synthesis of ZIFs from zinc and nickel nitrate solution for photocatalytic H2O2 production,” *Arabian Journal of Chemistry*, vol. 13, no. 11, pp. 8301–8308, Nov. 2020, doi: 10.1016/j.arabjc.2020.04.027.

[7] Z. Jiang, Y. Zhang, L. Zhang, B. Cheng, and L. Wang, “Effect of calcination temperatures on photocatalytic H2O2-production activity of ZnO nanorods,” *Chinese Journal of Catalysis*, vol. 43, no. 2, pp. 226–233, Feb. 2022, doi: 10.1016/S1872-2067(21)63832-9.

[8] C. Samanta, “Direct synthesis of hydrogen peroxide from hydrogen and oxygen: An overview of recent developments in the process,” *Appl Catal A Gen*, vol. 350, no. 2, pp. 133–149, Nov. 2008, doi: 10.1016/j.apcata.2008.07.043.

[9] L. Pi *et al.*, “Generation of H2O2 by on-site activation of molecular dioxygen for environmental remediation applications: A review,” *Chemical Engineering Journal*, vol. 389, p. 123420, Jun. 2020, doi: 10.1016/j.cej.2019.123420.

[10] H. Kim, Y. Choi, S. Hu, W. Choi, and J.-H. Kim, “Photocatalytic hydrogen peroxide production by anthraquinone-augmented polymeric carbon nitride,” *Appl Catal B*, vol. 229, pp. 121–129, Aug. 2018, doi: 10.1016/j.apcatb.2018.01.060.

[11] G. Gao, Y. Tian, X. Gong, Z. Pan, K. Yang, and B. Zong, “Advances in the production technology of hydrogen peroxide,” *Chinese Journal of Catalysis*, vol. 41, no. 7, pp. 1039–1047, Jul. 2020, doi: 10.1016/S1872-2067(20)63562-8.

[12] C. Byrne, G. Subramanian, and S. C. Pillai, “Recent advances in photocatalysis for environmental applications,” *J Environ Chem Eng*, vol. 6, no. 3, pp. 3531–3555, Jun. 2018, doi: 10.1016/j.jece.2017.07.080.

[13] S. Khan *et al.*, “Degradation of Congo red dye using ternary metal selenide-chitosan microspheres as robust and reusable catalysts,” *Environ Technol Innov*, vol. 22, p. 101402, May 2021, doi: 10.1016/j.eti.2021.101402.

[14] K. Nakata and A. Fujishima, “TiO2 photocatalysis: Design and applications,” *Journal of Photochemistry and Photobiology C: Photochemistry Reviews*, vol. 13, no. 3, pp. 169–189, Sep. 2012, doi: 10.1016/j.jphotochemrev.2012.06.001.

[15] M. Thomas, G. A. Naikoo, M. U. D. Sheikh, M. Bano, and F. Khan, “Effective photocatalytic degradation of Congo red dye using alginate/carboxymethyl cellulose/TiO2 nanocomposite hydrogel under direct sunlight irradiation,” *J Photochem Photobiol A Chem*, vol. 327, pp. 33–43, Aug. 2016, doi: 10.1016/j.jphotochem.2016.05.005.

[16] D. Ljubas, G. Smoljanić, and H. Juretić, “Degradation of Methyl Orange and Congo Red dyes by using TiO2 nanoparticles activated by the solar and the solar-like radiation,” *J Environ Manage*, vol. 161, pp. 83–91, Sep. 2015, doi: 10.1016/j.jenvman.2015.06.042.

[17] C. Sambathkumar, V. Manirathinam, A. Manikandan, M. Krishna Kumar, S. Sudhahar, and P. Devendran, “Solvothermal synthesis of Bi2S3 nanoparticles for active photocatalytic and energy storage device applications,” *Journal of Materials Science: Materials in Electronics*, vol. 32, no. 15, pp. 20827–20843, Aug. 2021, doi: 10.1007/s10854-021-06596-w.

[18] Y. S. Chaudhary *et al.*, “Visible light-driven CO_2 reduction by enzyme coupled CdS nanocrystals,” *Chem. Commun.*, vol. 48, no. 1, pp. 58–60, 2012, doi: 10.1039/C1CC16107E.

[19] M. S. Reza, N. B. H. Ahmad, S. Afroze, J. Taweekun, M. Sharifpur, and A. K. Azad, “Hydrogen Production from Water Splitting through Photocatalytic Activity of Carbon-Based Materials,” *Chem Eng Technol*, vol. n/a, no. n/a, doi: https://doi.org/10.1002/ceat.202100513.

[20] H. Dong *et al.*, “An overview on limitations of TiO2-based particles for photocatalytic degradation of organic pollutants and the corresponding countermeasures,” *Water Res*, vol. 79, pp. 128–146, Aug. 2015, doi: 10.1016/j.watres.2015.04.038.

[21] J. A. Nasir, Z. ur Rehman, S. N. A. Shah, A. Khan, I. S. Butler, and C. R. A. Catlow, “Recent developments and perspectives in CdS-based photocatalysts for water splitting,” *J Mater Chem A Mater*, vol. 8, no. 40, pp. 20752–20780, 2020, doi: 10.1039/D0TA05834C.

[22] K. Chatterjee and S. E. Skrabalak, “Durable Metal Heteroanionic Photocatalysts,” *ACS Appl Mater Interfaces*, vol. 13, no. 31, pp. 36670–36678, Aug. 2021, doi: 10.1021/acsami.1c09774.

[23] M. Yaghoubi-berijani and B. Bahramian, “Synthesis, and New Design into Enhanced Photocatalytic Activity of Porphyrin Immobilization on the Surface of Bismuth Oxyhalides Modified with Polyaniline,” *J Inorg Organomet Polym Mater*, vol. 30, no. 11, pp. 4637–4654, Nov. 2020, doi: 10.1007/s10904-020-01652-0.

[24] Y. Moriya, T. Takata, and K. Domen, “Recent progress in the development of (oxy)nitride photocatalysts for water splitting under visible-light irradiation,” *Coord Chem Rev*, vol. 257, no. 13–14, pp. 1957–1969, Jul. 2013, doi: 10.1016/j.ccr.2013.01.021.

[25] K. Maeda, T. Takata, and K. Domen, “(Oxy)nitrides and Oxysulfides as Visible-Light-Driven Photocatalysts for Overall Water Splitting,” 2011, pp. 487–529. doi: 10.1007/978-0-85729-638-2_14.

[26] T. Takata, C. Pan, and K. Domen, “Recent progress in oxynitride photocatalysts for visible-light-driven water splitting,” *Sci Technol Adv Mater*, vol. 16, no. 3, p. 033506, Jun. 2015, doi: 10.1088/1468-6996/16/3/033506.

[27] Q. Wang *et al.*, “Oxysulfide photocatalyst for visible-light-driven overall water splitting,” *Nat Mater*, vol. 18, no. 8, pp. 827–832, Aug. 2019, doi: 10.1038/s41563-019-0399-z.

[28] K. Huang, Y. Li, and Y. Xing, “Carbothermal synthesis of titanium oxycarbide as electrocatalyst support with high oxygen evolution reaction activity,” *J Mater Res*, vol. 28, no. 3, pp. 454–460, Feb. 2013, doi: 10.1557/jmr.2012.353.

[29] D. Lopes *et al.*, “Design of Multifunctional Titania-Based Photocatalysts by Controlled Redox Reactions,” *Materials*, vol. 13, no. 3, p. 758, Feb. 2020, doi: 10.3390/ma13030758.

[30] J. Cuan *et al.*, “Multiple Anionic Transition-Metal Oxycarbide for Better Lithium Storage and Facilitated Multielectron Reactions,” *ACS Nano*, vol. 13, no. 10, pp. 11665–11675, Oct. 2019, doi: 10.1021/acsnano.9b05580.

[31] K. Huang, Y. Li, and Y. Xing, “Carbothermal synthesis of titanium oxycarbide as electrocatalyst support with high oxygen evolution reaction activity,” *J Mater Res*, vol. 28, no. 3, pp. 454–460, Feb. 2013, doi: 10.1557/jmr.2012.353.

[32] S. Guan, L. Hao, H. Yoshida, F. Pan, H. Asanuma, and Y. Lu, “Enhanced photocatalytic activity of photocatalyst coatings by heat treatment in carbon atmosphere,” *Mater Lett*, vol. 167, pp. 43–46, Mar. 2016, doi: 10.1016/j.matlet.2015.12.074.

[33] B. Chong, H. Li, B. Xu, and G. Yang, “Hollow double-shell stacked CdS@ZnIn2S4 photocatalyst incorporating spatially separated dual cocatalysts for the enhanced photocatalytic hydrogen evolution and hydrogen peroxide production,” *Catal Today*, vol. 405–406, pp. 227–234, Dec. 2022, doi: 10.1016/j.cattod.2022.05.020.

[34] Y. Wei, J. Zhang, Q. Zheng, J. Miao, PedroJ. J. Alvarez, and M. Long, “Quantification of photocatalytically-generated hydrogen peroxide in the presence of organic electron donors: Interference and reliability considerations,” *Chemosphere*, vol. 279, p. 130556, Sep. 2021, doi: 10.1016/j.chemosphere.2021.130556.

[35] E. Zhang *et al.*, “Visually resolving the direct Z-scheme heterojunction in CdS@ZnIn2S4 hollow cubes for photocatalytic evolution of H2 and H2O2 from pure water,” *Appl Catal B*, vol. 293, p. 120213, Sep. 2021, doi: 10.1016/j.apcatb.2021.120213.

[36] B. Zhang, J. Xiao, S. Jiao, and H. Zhu, “A novel titanium oxycarbide phase with metal-vacancy (Ti1-C O1-): Structural and thermodynamic basis,” *Ceram Int*, vol. 47, no. 11, pp. 16324–16332, Jun. 2021, doi: 10.1016/j.ceramint.2021.02.212.

[37] B. Jiang *et al.*, “Structural studies of TiC1−xOx solid solution by Rietveld refinement and first-principles calculations,” *J Solid State Chem*, vol. 204, pp. 1–8, Aug. 2013, doi: 10.1016/j.jssc.2013.05.009.

[38] D. N. Miller *et al.*, “Studies on the crystal structure, magnetic and conductivity properties of titanium oxycarbide solid solution ($TiO_{1-x}C_x$),” *J Mater Chem A Mater*, vol. 4, no. 15, pp. 5730–5736, 2016, doi: 10.1039/C6TA00042H.

[39] Y. Subramanian *et al.*, “Investigations on the enhanced dye degradation activity of heterogeneous BiFeO3–GdFeO3 nanocomposite photocatalyst,” *Heliyon*, vol. 5, no. 6, p. e01831, Jun. 2019, doi: 10.1016/j.heliyon.2019.e01831.

[40] C. Negi *et al.*, “Carbon-doped titanium dioxide nanoparticles for visible light driven photocatalytic activity,” *Appl Surf Sci*, vol. 554, p. 149553, Jul. 2021, doi: 10.1016/j.apsusc.2021.149553.

[41] P. Kumar *et al.*, “Photocatalytic activity of a hydrothermally synthesized γ-Fe2O3@Au/MoS2 heterostructure for organic dye degradation under green light,” *J Photochem Photobiol A Chem*, vol. 433, p. 114186, Dec. 2022, doi: 10.1016/j.jphotochem.2022.114186.

[42] P. Apopei, C. Catrinescu, C. Teodosiu, and S. Royer, “Mixed-phase TiO2 photocatalysts: Crystalline phase isolation and reconstruction, characterization and photocatalytic activity in the oxidation of 4-chlorophenol from aqueous effluents,” *Appl Catal B*, vol. 160–161, pp. 374–382, Nov. 2014, doi: 10.1016/j.apcatb.2014.05.030.

[43] Y. Subramanian, B. Mishra, S. Mandal, R. Gubendiran, and Y. S. Chaudhary, “Design of heterostructured perovskites for enhanced photocatalytic activity: Insight into their charge carrier dynamics,” *Mater Today Proc*, vol. 35, pp. 179–185, 2021, doi: 10.1016/j.matpr.2020.04.215.

[44] Y. Subramanian, V. Ramasamy, R. K. Gubendiran, G. R. Srinivasan, and D. Arulmozhi, “Structural, Optical, Thermal and Photocatalytic Dye Degradation Properties of BiFeO3–WO3 Nanocomposites,” *J Electron Mater*, vol. 47, no. 12, pp. 7212–7223, Dec. 2018, doi: 10.1007/s11664-018-6654-2.

[45] X. Xie *et al.*, “Efficient photo-degradation of dyes using $CuWO_4$ nanoparticles with electron sacrificial agents: a combination of experimental and theoretical exploration,” *RSC Adv*, vol. 6, no. 2, pp. 953–959, 2016, doi: 10.1039/C5RA18788E.

[46] Y. Chen, W. Gu, L. Tan, Z. Ao, T. An, and S. Wang, “Photocatalytic H2O2 production using Ti3C2 MXene as a non-noble metal cocatalyst,” *Appl Catal A Gen*, vol. 618, p. 118127, May 2021, doi: 10.1016/j.apcata.2021.118127.